Nanoscale

Electrical and Thermal Conduction in Ultra-thin Freestanding Atomic Layer Deposited W Nanobridges

Nathan T. Eigenfeld[a], Jonas C. Gertsch[b], George D. Skidmore[c], Steven M. George[a,b], Victor M. Bright[a]

[a]Department of Mechanical Engineering, University of Colorado at Boulder, 1111 Engineering Drive, 427 UCB, Boulder, CO 80309-0427, USA.

[b]Department of Chemistry and Biochemistry and Department of Mechanical Engineering, University of Colorado at Boulder, 215 UCB Boulder, CO 80309-0215, USA

[c]DRS Technologies Inc., Network and Imaging Systems DRS ITS Texas Site, 13532 North Central Expwy SC Bldg, Dallas, TX 75243, USA

Abstract

Work presented here measures and interprets the electrical and thermal conductivities of atomic layer deposition (ALD) free-standing single film and periodic tungsten and aluminum oxide nanobridges with thicknesses from ~ 5 – 20 nm and ~ 3 – 13 nm, respectively. Electrical conductivity of the W films are reduced by up to 99% from bulk, while thermal conductivity is reduced by up to 91%. Results indicate phonon contribution to thermal conductivity is dominant in these ALD films and may be substantially reduced by the incorporation of periodicity in the ALD W/Al$_2$O$_3$ nanolaminates. Additionally, thin film conduciton modeling demonstrates nano-structured grain features largely dictate electron and phonon conduction in ALD W. New fabrication methods have allowed for the development of free-standing ultra-thin structures with layers on the order of several nanometers utilizing ALD. While the literature contains diverse studies of the physical properties of thin films prepared by traditional micro-fabrication sputtering or chemical vapor deposition techniques,

1

there remains little data on freestanding structures containing ALD generated materials. Specifically, knowledge of the electrical and thermal conductivity of ALD generated materials will aid in the future development of ultra-thin nano-devices.

Introduction

Exciting research with 2D nanomaterials such as graphene and carbon nanotubes and ultra-small structures such as nanowires and quantum dots is highly relevant to the future of nano-electronics and nano-engineering.[1–7] However, there remains little characterization of ultra-thin metal/metal oxide thin film laminates, which are more easily implemented as electrical or thermal interconnects into current micro-fabrication techniques. Specifically, the study of ultra-thin suspended structures for use in nano and micro electro-mechanical systems (N/MEMS) is becoming increasingly relevant.[8] Past micro-fabrication methods have made suspension of thin films with thicknesses on the order of 10 nm's challenging. Since many thermal measurements require suspended structures to minimize thermal loss to underlying substrates, there has been little characterization of ultra-thin films' thermal properties for use in nano-devices.[8–11] However, with recent developments in fabrication processes combining the use of atomic layer deposition (ALD) ultra-thin films and polymer based micro-machining, structures with sub-20 nm thicknesses are easily fabricated.[12] This process is highly beneficial to the future characterization of many ultra-thin suspended films. Studies of these films often illuminate drastic physical property differences in the films from bulk. For example, electrical properties may vary substantially at the nanoscale due to an increased amount of electron scattering at film boundaries, grain boundaries and impurities or defects.[13] The knowledge of these differences will no doubt benefit the nano-engineering community through enhanced design and modeling of future nano-devices.

This work reports on the measurement of the electrical conductivity and thermal conductivity of freestanding tungsten (W) and aluminum oxide (Al_2O_3), and periodic
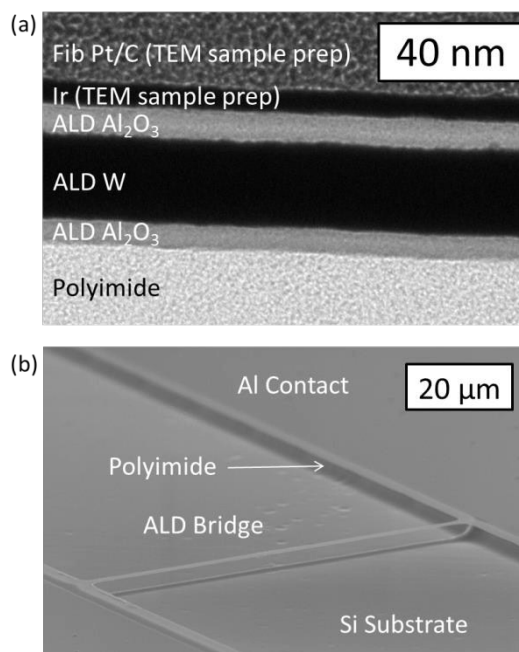
Figure 1. TEM cross-section and SEM image of test structures. a) TEM cross-section image of Al_2O_3/W/Al_2O_3 coating on polyimide with similar thickness to the test structures.[12] b) SEM image tilted by 75° of an 80 x 2 μm^2 suspended bridge of 3.2 nm Al_2O_3/20.40 nm W/3.2 nm Al_2O_3 with Al contact pads.

W/Al_2O_3 nanobridges at 300 K. The film thicknesses of both W and Al_2O_3 were varied between ~ 5 – 20 nm and ~ 3 – 13 nm, respectively, and fabricated using an ALD on polyimide process developed by the authors.[12] Figure 1 demonstrates a cross-sectional TEM image of a characteristic Al_2O_3/W/Al_2O_3 nanolaminate and a fabricated nanobridge with electrical contact pads. ALD is a thin film deposition method which uses a self-limiting binary reaction sequence that deposits films in discrete steps limited by surface site chemical reactions.[14,15] It typically produces continuous pinhole-free films with atomically controlled thicknesses, high conformality, and atomically smooth surfaces. These are essential properties as design constraints push device technologies to ever smaller sizes.[16,17] For example, recent work with ALD materials have involved the fabrication of ALD Pt microbolometers and an array of various N/MEMS devices involving ALD Al_2O_3, ALD W/Al_2O_3 and ALD Ru/Al_2O_3.[8,12,18–24] Thermal barrier research has involved the characterization of through-plane interface thermal resistance in ALD W/Al_2O_3 coatings, however, specific studies of the
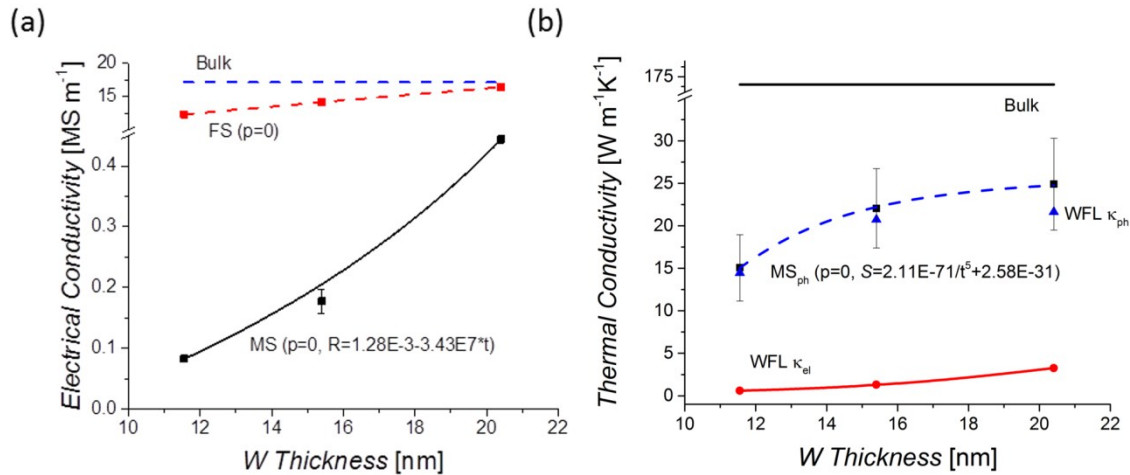
3

Figure 2. Measured electrical and thermal conductivity of W films at 300 K at three thicknesses are plotted as black squares. a) The bulk W conductivity is shown as the blue dashed line. The lower bound FS model (p=0) is shown as the red dashed line. The solid black line is the thickness dependent MS model. b) The black line is the bulk value. The red circles are WFL calculated κ_{el} values. The blue triangles are WFL calculated κ_{ph} values. The blue dashed line is the thickness dependent MS_{ph} model. The blue triangles are WFL calculated κ_{ph} values. The blue dashed line is the thickness dependent MS_{ph} model.

electrical and thermal conduction properties of freestanding ALD W/Al_2O_3 nanolaminates remains absent in the literature.[25]

Results

Figure 2a demonstrates the electrical conductivity of three W thicknesses (11.55, 15.40 and 20.40 nm) at 300 K. The electrical conductivity of ALD W is significantly smaller than bulk values and varies considerably with thickness. It is generally understood that thin films will exhibit smaller conductivity than bulk materials due to sizing effects. This effect is often modeled using Fuchs-Sondheimer (FS) theory, which considers size effects in thin films by accounting for the fraction of specular or diffuse electron scattering at film boundaries with the constant p.[26,27] The ratio of film conductivity relative to bulk is given as,

$$\frac{\sigma}{\sigma_o}=1-\frac{3(1\text{-}p)}{8\lambda}+\frac{3}{4\lambda}\int_0^{\pi}\sin^3\theta|\cos\theta|\frac{(1\text{-}p)^2\exp(-\frac{\lambda}{|\cos\theta|})}{1\text{-}p\cdot\exp(-\frac{\lambda}{|\cos\theta|})}d\theta,$$ (1)

4

where λ is equal to the film thickness divided by the electron mean free path.[26] Even for

completely diffuse scattering (p = 0), the FS model drastically overshoots the experimental W

conductivity. Since the W is nanocrystalline, the data are more accurately modeled by using

the Mayadas-Shatzkes (MS) model (black solid line in Figure 2a), which takes into account

electron scattering at grain boundaries or impurities through an electron reflection coefficient

R.[15,28] The full model incorporates both the Fuch's size effect and grain boundary scattering,

but for the case of negligible sizing effects relative to the grain boundary resistivity

contributions, a simplified model may be utilized. The grain boundary conductivity model is

given as,

$$\frac{\sigma}{\sigma_o}=3\left[\frac{1}{3}-\frac{1}{2}\alpha+\alpha^2-\alpha^3\ln\left(1+\frac{1}{\alpha}\right)\right], \tag{2}$$

where α relates the grain boundary potential strength by,

$$\alpha=\frac{l_o}{G}\frac{R}{1-R}, \tag{3}$$

where l_o is the electron mean free path in the bulk material, G is the grain size and R is the

electron reflection coefficient for a grain boundary.[28] For a thickness independent constant

grain size of ~ 2 nm that has been confirmed by XRD analysis for these films (see supporting

information), a thickness-dependent electron reflection coefficient, R, must be utilized to

properly fit the data. Previous work with ALD Pt films explained this thickness dependent R

value through the concept of varied density with Pt thickness, however, nucleation studies of

ALD W show a constant density at the thicknesses studied.[8,15] The thickness dependent effect

for R is likely attributed to a disordered layer formed during the recrystallization of grains in

the W nucleation phase.[15] A base layer of disordered grains could result in more electron

scattering for thinner films, increasing R. This hypothesis is supported by the measurement of

a negative temperature coefficient of resistance (TCR) for ALD W, opposite of the expected

positive metallic effect. Specifically, thinner films exhibit a larger negative TCR with

measured values of -0.015, -0.012 and -0.009 % K^{-1} for 11.55, 15.40 and 20.40 nm W films,
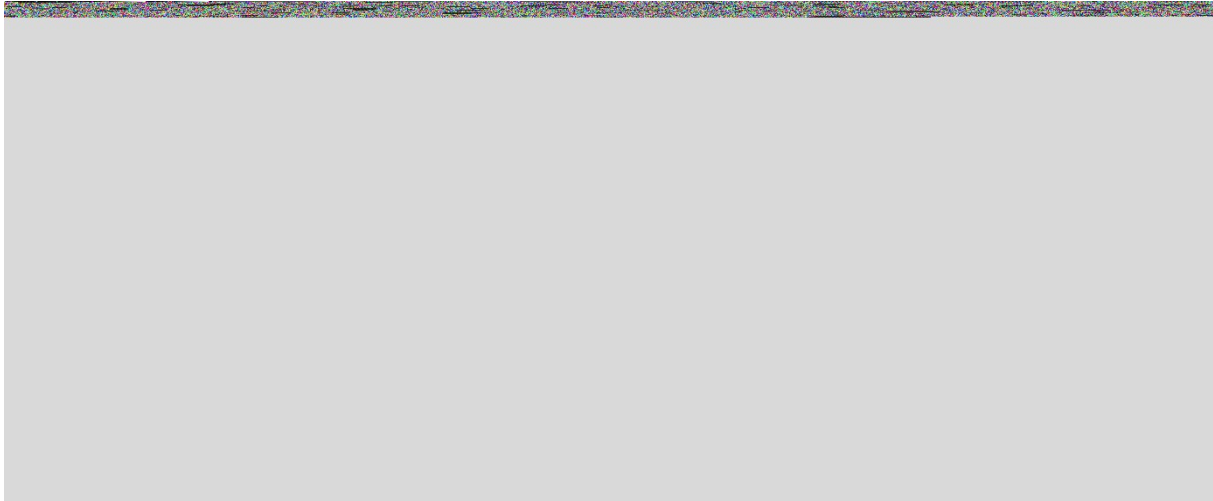
Figure 2. Measured electrical and thermal conductivity of W films at 300 K at three thicknesses are plotted as black squares. a) The bulk W conductivity is shown as the blue dashed line. The lower bound FS model (p=0) is shown as the red dashed line. The solid black line is the thickness dependent MS model. b) The black line is the bulk value. The red circles are WFL calculated κ_{el} values. The blue triangles are WFL calculated κ_{ph} values. The blue dashed line is the thickness dependent MS_{ph} model. The blue triangles are WFL calculated κ_{ph} values. The blue dashed line is the thickness dependent MS_{ph} model.

respectively. Thinner films contain a larger scattering contribution from the disordered nucleation layer which contributes a negative TCR effect through electron grain hopping. These negative TCR contributions overcome the inter-grain metallic positive TCR contribution.

Figure 2b demonstrates the measured effective thermal conductivity of the same W thicknesses from Figure 2a. The error bars in Figure 2b are 95% confidence intervals. The majority of this error is attributed to the thermal conductance fitting procedure and error propogation into the thermal conductivity extraction. Error in Al_2O_3 and W thicknesses, and error in nanobridge widths are also included. Given these W films have a substantially lower electrical conductivity than bulk, the electron thermal conductivity κ_{el} (solid red line in Figure 2b) will be reduced substantially following the Weidemann-Franz Law (WFL). However, the 3.2 nm amorphous Al_2O_3 capping layers surrounding the W will contribute some degree of phonon conduction given they have a thermal conductivity of ~ 1 – 2.5 W m^{-1} K^{-1}.[25,29,30] A parallel conduction model to include the Al_2O_3 contribution to the total conduction and extract

the contribution from just the W layer was used. Work from Gorham et al. measured a thermal conductivity for ALD Al_2O_3 films with similar growth conditions and density of 1.5 W m^{-1} K^{-1}.[29] This value was used in the extraction of the W thermal conductivity from the trilayer stack.

The calculated Lorenz numbers L based on the measured thermal and electrical conductivities of the W films are 6.07×10^{-7}, 4.15×10^{-7} and 1.87×10^{-7} for 11.55, 15.40 and 20.40 nm thicknesses. These values are significantly larger than the Sommerfeld value $L_o = 2.45 \times 10^{-8}$ obtained by the free electron theory of metals. The electron thermal conductivity κ_e was calculated using the WFL $\kappa_e = L_oT\sigma$ where T is the absolute temperature and σ is the measured electrical conductivity and compared to the measured thermal conductivity of W (Figure 2b). The large disparity between the measured thermal conductivity and the calculated κ_e is due to a large contribution from phonon conduction. Reflected electrons at grain boundaries may exchange energy with local phonons, which will then trasfer energy across the grain boundary. The thermal conduction in ALD W is dominated by phonon conduction (triangle data points in Figure 2b) since the total conductivity is the sum of electron and phonon conductivities.

A modified MS model for phonon conduction was fit to the WFL calculated phonon conduction (dashed line in Figure 2b).[31] Similar to R in the electrical MS model, there is an analogous term S_{ph} that represents the strength of a grain boundary potential that may scatter phonons. The film thermal conductivity is given as,

$$\kappa_{ph}=\kappa_{ph,bulk}g_{ph}(d,G), \tag{4}$$

where $\kappa_{ph,bulk}$ is the bulk material thermal conductivity and $g_{ph}(d,G)$ is given as,

$$g_{ph}(d,G)=\frac{\int_0^{\Theta/T}\frac{x^4e^x}{(e^x-1)^2}\tau_q(x)\left\{1+\frac{3}{2}\gamma+\frac{3(1-p_{ph})}{8K}\right\}^{-1}dx}{\int_0^{\Theta/T}\frac{x^4e^x}{(e^x-1)^2}\tau_q(x)dx}, \tag{5}$$

with $\quad \gamma = \frac{2S_{ph}^2 \tau_q(x)}{\hbar^2 vG}, \qquad\qquad x = \frac{\hbar\omega}{k_b T}, \qquad\qquad K = \frac{d}{\tau_q(x)v}.$ [31]

For the above relations, τ_q is the phonon-phonon umklapp scattering relaxation time, ω is the Debye frequency, v is the sound velocity, Θ is the Debye temperature, p_{ph} is the parameter of surface scattering. The umklapp scattering relaxation time may be modeled as[32],

$$\tau_q(\omega) = {\tau_{u0}}/{k_B T \omega^2} \; , \tag{6}$$

and applied to Equation 5 to obtain the following relation,

$$g_{ph}(d,G) \approx \frac{\int_0^{\Theta/T} \frac{x^2 e^x}{(e^x-1)^2}\left(1+\frac{\gamma_1}{x^2}+\frac{\gamma_2}{x^2}\right)dx}{\int_0^{\Theta/T} \frac{x^2 e^x}{(e^x-1)^2}dx} \; , \tag{7}$$

where $\quad \gamma_1 = \frac{3S_{ph}^2 \tau_{u0}}{vG(k_b T)^3}, \quad \gamma_2 = \frac{3\left(1-p_{ph}\right)v\tau_{u0}\hbar^2}{8d(k_b T)^3}.$

Here, τ_{u0} and S_{ph} become fitting parameters for g_{ph}, where g_{ph} must be solved numerically. For a fixed value of $\tau_{u0} = 10^{-5}$ from prior literature on Bismuth and Antimony films[31], W bulk conductivity of 173 W m^{-1} K^{-1}, W Debye temperature of 400 K, W Debye frequency of 80,800 GHz, W phonon velocity of 5180 m s^{-1}, grain size of 2 nm, and a completely diffuse film boundary scattering term $p_{ph} = 0$, a thickness dependent S_{ph} term must be utilized to accurately fit the data. Analogous to the electrical conductivity thickness dependent R term there is likely a disordered base nucleation layer within the W, which has a larger relative effect on thinner films. Overall, the thermal conductivity was reduced ~ 91% from bulk for the 11.55 nm W thickness.

The periodicity dependence of thermal conductivity for thin suspended nanolaminates with a total W and Al$_2$O$_3$ thickness of 20.40 nm and 13 nm is demonstrated in Figure 3a. Figure 3b demonstrates the cross-section of these periodic laminates from one to four layers of W with a constant total thickness. While laminates and superlattices are common approaches to the optimization of out of plane electrical and thermal conduction in thermoelectric materials, they may also benefit suspended nano-devices which conduct
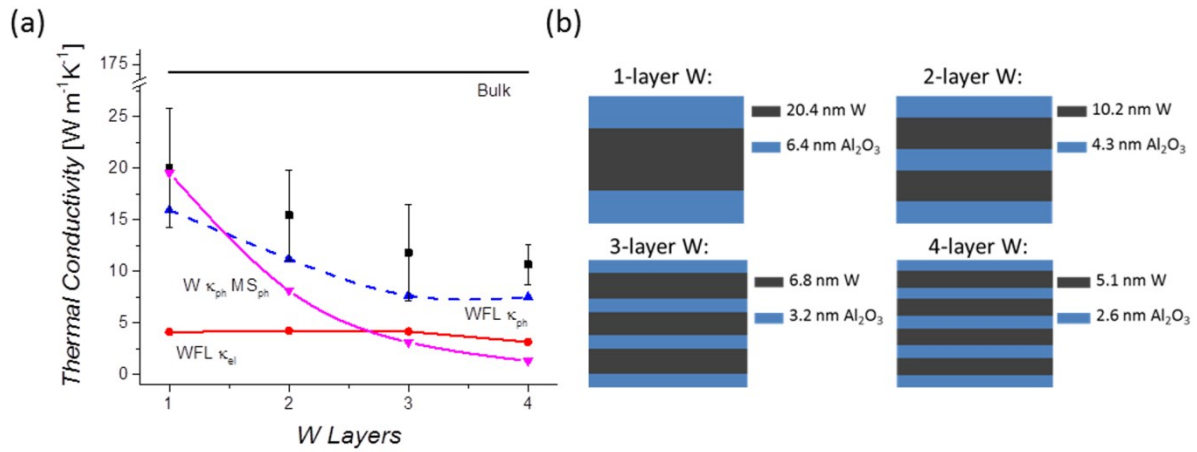
8

Figure 3. Periodic W/Al$_2$O$_3$ nanobridges. a) The periodicity dependent thermal conductivity of W/Al$_2$O$_3$ laminates are plotted as black squares. One – four layers denote the number of layers the W is split into with equal thickness Al$_2$O$_3$ spacers and maintaining constant total thickness (b). The black line is the bulk value. The red circles are WFL calculated κ_{el}. The blue triangles are WFL calculated κ_{ph}. The upside-down purple triangles are values modeled by the MS$_{ph}$ model using the same thickness dependent S term from Figure 2b. b) Periodic nanolaminate cross-sections.

electricity and heat in-plane.[25] Phonon conduction was reduced by introducing periodicity into the W film with Al$_2$O$_3$ spacers while keeping the total thickness constant. For example, a four layer W film consists of a laminate of four 5.05 nm W films split up by five 2.6 nm Al$_2$O$_3$ spacers. The electrical conductivity of the periodic films remained relatively constant when splitting up the W, therefore the reduction in total thermal conductivity can be attributed to a reduction in phonon conduction. Interfacial thermal resistance, or boundary resistance is likely invoking further scattering processes which reduce phonon conduction in both the individual W and Al$_2$O$_3$ layers and across the interfacial boundaries. This effect will likley increase as the layer number increases. For a constant total thickness of W and Al$_2$O$_3$, the total thermal conductivity was reduced ~ 47% by introducing periodicity. By ignoring the small conduction contribution of the Al$_2$O$_3$ spacers the W conduction may be modeled as parallel conductors where the total thermal conductivity is,

$$\kappa_{tot} = \sum_{i=1}^{N} \kappa_{W,i} t_{W,i}/t_{W,tot} = N\kappa_{W,N} t_{W,N}/t_{W,tot}, \qquad (8)$$

where i denotes an individual W layer with thickness $t_{W,i}$ and thermal conductivity $\kappa_{W,i}$, and $t_{W,tot}$ is the total W thickness. Since the individual W layers have equal thicknesses,

9

Table 1. Summary of electrical and thermal properties of W and W/Al$_2$O$_3$ periodic films.

W Sample	σ [MSm^{-1}]	ρ [$\mu\Omega$m^{-1}]	κ [Wm^{-1}K^{-1}]	R_λ [mKW^{-1}]
11.6 nm	0.08	12.08	15.1	0.066
15.4 nm	0.18	5.64	22.1	0.045
20.4 nm	0.44	2.25	24.9	0.040
1-layer	0.44	2.25	20.0	0.05
2-layer	0.45	2.20	15.4	0.06
3-layer	0.45	2.20	11.8	0.08
4-layer	0.34	2.90	10.7	0.09
Bulk	17.2	0.06	173	0.006

$$t_{W,i}/t_{W,tot}=1/N, \tag{9}$$

and thus, κ_{tot} becomes the conductivity of an individual W film, $\kappa_{W,i}$ within the laminate. Utilizing the same thickness dependent S_{ph} used to fit the data from Figure 2b, the phonon thermal conductivity of the W in the periodic structure was modeled using the MS model modified for phonon conduction (solid inverted triangles Fig. 3a).[31] The model demonstrates that phonon conduction in the W is reduced substantially. However, this model is not a completely accurate description of the thermal conductivity of the laminate since the sum of the MS model phonon conductivity and WFL electron conductivity from the W is several W m^{-1} K^{-1} less than the total measured thermal conductivity of the laminate for the 3 and 4 layer samples. This error is attributed to the lack of consideration for Al$_2$O$_3$ conduction since the phonon conduction from both the W and Al$_2$O$_3$ are on the same order of magnitude for the 3 and 4 layer samples. Also, nucleation effects from the W may be incorporating additional error effects since the nucleation phase is a larger portion of each total deposition cycle for thinner W layers in the more periodic structures.[15]

Table 1 summarizes the electrical conductivities, electrical resistivities (ρ), thermal conductivities and thermal resistivities (R_λ) of the three single layer W thicknesses, four periodic samples (Figure 3b) and the bulk values. Within the thickness range studied for single layer W films, the W loses electrical conductivity faster than thermal conductivity with decreasing film thickness. Within the range of periodicity studied, the W loses thermal

10

conductivity faster than electrical conductivity with increasing periodicity. These trends may be exploited in future designs of freestanding nano-devices with particular requirements for electrical and thermal conduction.

Experimental Section

Nanobridge fabrication: A thorough overview of the general fabrication process is outlined in previous work by the authors, however a brief overview will be provided here.[12,33] First, a thin sacrificial layer of polyimide is spun-on and cured on a bare Si wafer to a thickness of ~ 3 μm. Then an amorphous film of Al_2O_3 is deposited by ALD at 130 °C using trimethylaluminum (TMA) and H_2O as gas precursors for growth at ~ 0.13 nm/cycle. This initial Al_2O_3 layer aids in the nucleation of the following W layer, which is also deposited at 130 °C and uses Si_2H_6 and WF_6 as gas precursors for growth at ~ 0.38 nm/cycle.[15,34] Finally, another Al_2O_3 film is deposited to encapsulate the W, protecting it from oxidizing. All layers are patterned using reactive ion etching. Contact pads are formed by evaporation of Al and lift-off patterning. The final structures are released by removing the polyimide in an oxygen plasma process. ALD cycles determine the discrete thickness of the W and Al_2O_3. Thicknesses were verified by TEM and prior knowledge of deposition rates using X-ray reflectivity (XRR).[15,34]

Electrical and thermal measurement process: The electrical and thermal conductivities are measured separately during different stages of fabrication. The electrical resistances of an array of nanobridge lengths are measured using a four probe configuration pre-release with a maximum bias current of 10 μA to minimize Joule heating. Next, electrical conductivity is extracted through a fit of resistance versus length, following the relation:

$$R = {L}/{\sigma A}, \tag{10}$$

where R is the resistance of the beam, L the length, A the beam cross-sectional area, and σ the electrical conductivity. Additionally, the average TCR of ~14 beams per sample is measured pre-release upon a heated stage at various temperatures with a maximum of 10 μA bias current (shortest and lowest resistance bridges) to minimize Joule heating. The TCR is measured over a 100 K temperature increase using a four probe configuration. The thermal conductances of an array of beam lengths are measured post-release using steady-state DC Joule heating under vacuum at ~ 30 mTorr. The power applied and the resulting change in resistance are monitored by four probe voltage-current measurements. Resistance change is converted to temperature through TCR, and thermal conductance, G_{th}, is extracted by fitting power applied to the beam versus its change in temperature. Maximum change in temperatures are limited to ~100 K. Thermal conductivity is extracted by solving the 1-D heat equation for the case of Joule heating and fitting the thermal conductance versus beam length through the following relation:

$$G_{th} = {12 \, \kappa \, A}/{L} , \tag{11}$$

where κ is the effective in-plane thermal conductivity of the ALD nanolaminate. Calculated effects from conduction to air and thermal radiation only result in ~ 2% shift in the thermal conductivity.[35] The accuracy of the thermal loss calculations were verified by comparing thermal conductance measurements at 30 mTorr and 500 μTorr. The accuraracy of the measurement technique was validated by measuring a 100 nm Aluminum. A value of 210 ± 5 W/mK was obtained, agreeing within ~ 1.5% of the value of ~ 214 W/mK obtained in previous studies by Volkov et al..[36]

Conclusion

Electrical and thermal conductivities of freestanding ALD deposited $Al_2O_3/W/Al_2O_3$ and periodic $Al_2O_3/W/Al_2O_3$ nanolaminates have been measured at 300 K. The traditional FS model fails to describe the electrical properties of nano-crystalline ALD W. The electrical and

phonon adapted MS model for W both incorporate a thickness dependent grain boundary scattering term, likely attributed to a highly disordered base layer formed during the ALD nucleation phase, which has a stronger effect on thinner films. Phonon conduction dominates the thermal conductivity of the W, but can be substantially reduced by incorporating periodicity in the W film. Utilizing this method may allow the fabrication of freestanding ultra-thin films that have approximately zero phonon conduction and have reached the WFL limit for conduction in a metal film – an interesting utility for future nano-engineering.

Electronic Supplementary Information

Electronic supplementary information (ESI) is available online. This information outlines examples of thermal conductance measurements, thermal conductivity extraction, accuracy of the measurement method and thermal loss calculations and adjustments. Also, discussion of XRD film analysis and ALD grain size is included.

Acknowledgements

1   K. C. Yung, W. M. Wu, M. P. Pierpoint, F. V. Kusmartsev, *Contemp. Phys.* 2013, **54**, 233.

2   M. F. El-Kady, R. B. Kaner, *ACS Nano* 2014, **8**, 8725.

3   S. P. Koenig, L. Wang, J. Pellegrino, J. S. Bunch, *Nat. Nanotechnol.* 2012, **7**, 728.

4   A. Vijayaraghavan, *Phys. Status Solidi B* 2013, **250**, 2505.

5   M. De Volder, S. H. Tawfick, S. J. Park, D. Copic, Z. Zhao, W. Lu, A. J. Hart, *Adv. Mater.* 2010, **22**, 4384.

6   K. Dohnalová, T. Gregorkiewicz, K. Kůsová, *J. Phys.: Condens. Matter* 2014, **26**, 173201.

7   S. G. Li, Q. Gong, C. F. Cao, X. Z. Wang, J. Y. Yan, Y. Wang, H. L. Wang, *Opt. Quantum Electron.* 2014, **46**, 623.

8   S. Yoneoka, J. Lee, M. Liger, G. Yama, T. Kodama, M. Gunji, J. Provine, R. T. Howe, K. E. Goodson, T. W. Kenny, *Nano Lett.* 2012, **12**, 683.

9   K. E. Petersen, *Proc. IEEE* 1982, **70**, 420.

10   P. J. French, *J. Micromech. Microeng.* 1996, **6**, 197.

11   H. Lin, S. Xu, X. Wang, N. Mei, *Small* 2013, **9**, 2585.

12   N. T. Eigenfeld, J. M. Gray, J. J. Brown, G. D. Skidmore, S. M. George, V. M. Bright, *Adv. Mater.* 2014, **26**, 3962.

13   A. J. Learn, D. W. Foster, *J. Appl. Phys.* 1985, **58**, 2001.

14   S. M. George, *Chem. Rev.* 2010, **110**, 111.

15   R. W. Wind, F. H. Fabreguette, Z. A. Sechrist, S. M. George, *J. Appl. Phys.* 2009, **105**, 074309.

16   G. K. Dalapati, Yi Tong, Wei-Yip Loh, Hoe Keat Mun, Byung Jin Cho, *IEEE Trans. Electron Devices* 2007, **54**, 1831.

17   M. Knaut, M. Junige, V. Neumann, H. Wojcik, T. Henke, C. Hossbach, A. Hiess, M. Albert, J. W. Bartha, *Microelectron. Eng.* 2013, **107**, 80.

18   F. Purkl, T. S. English, G. Yama, J. Provine, A. K. Samarao, A. Feyh, B. Kim, G. O'Brien, O. Ambacher, R. T. Howe, *Proc. TRANSDUCERS 2013 Eurosensors XXVII, 17th Conf. Solid-State Sens. Actuators Microsyst.* 2013, 1507.

19   B. D. Davidson, D. Seghete, S. M. George, V. M. Bright, *Sens. Actuators A.* 2011, **166**, 269.

20   Y.-J. Chang, J. M. Gray, A. Imtiaz, D. Seghete, T. Mitch Wallis, S. M. George, P. Kabos, C. T. Rogers, V. M. Bright, *Sens. Actuators A.* 2009, **154**, 229.

21   N. D. Hoivik, J. W. Elam, R. J. Linderman, V. M. Bright, S. M. George, Y. C. Lee, *Sens. Actuators A.* 2003, **103**, 100.

22   C. F. Herrmann, F. W. DelRio, D. C. Miller, S. M. George, V. M. Bright, J. L. Ebel, R. E. Strawser, R. Cortez, K. D. Leedy, *Sens. Actuators A.* 2007, **135**, 262.

23   M. K. Tripp, C. Stampfer, D. C. Miller, T. Helbling, C. F. Herrmann, C. Hierold, K. Gall, S. M. George, V. M. Bright, *Sens. Actuators A.* 2006, **130-131**, 419.

24   J. M. Gray, J. P. Houlton, J. C. Gertsch, J. J. Brown, C. T. Rogers, S. M. George, V. M. Bright, *J. Micromech. Microeng.* 2014, **24**, 125028.

25   R. M. Costescu, *Science* 2004, **303**, 989.

26   K. Fuchs, N. F. Mott, *Math. Proc. Cambridge Philos. Soc.* 1938, **34**, 100.

27   E. H. Sondheimer, *Adv. Phys.* 2001, **50**, 499.

28   A. F. Mayadas, M. Shatzkes, *Phys. Rev. B* 1970, **1**, 1382.

29   C. S. Gorham, J. T. Gaskins, G. N. Parsons, M. D. Losego, P. E. Hopkins, *Appl. Phys. Lett.* 2014, **104**, 253107.

30   Z. Luo, H. Liu, B. T. Spann, Y. Feng, P. Ye, Y. P. Chen, X. Xu, *Nanoscale Microscale Thermophys. Eng.* 2014, **18**, 183.

31   F. Voelklein, T. Franke, in *Therm. Conduct. 23*, CRC Press, 1996, pp. 129–144.

32   P. G. Klemens, in *Therm. Conduct.*, Academic Press, London, 1969.

33   N. T. Eigenfeld, B. J. Joseph, J. M. Gray, G. D. Skidmore, V. M. Bright, S. M. George, *US Application No.* 14 604 906, 2014.

34   C. A. Wilson, R. K. Grubbs, S. M. George, *Chem. Mater.* 2005, **17**, 5625.

35   M. M. Sisto, S. García-Blanco, L. Le Noc, B. Tremblay, Y. Desroches, J.-S. Caron, F. Provencal, F. Picard, in *SPIE* (Eds: R.C. Kullberg, R. Ramesham), 2010, pp. 759204–759204–10.

36   Y. A. Volkov, L. S. Palatnik and A. T. Pugachev, *Zh. Eksp. Teor. Fiz*, 1976, **70**, 2244–2250.